*Geophysical Fluid Dynamics.* 1970. Vol. 1, pp. 357–369

Printed in Great Britain

# Axisymmetric Annulus Convection at Unit Prandtl Number

GARETH P. WILLIAMS

Geophysical Fluid Dynamics Laboratory/ESSA
Princeton University
P.O. Box 308
Princeton, New Jersey 08540

*Received September* 15, 1969

**Abstract**—We examine the role played in annulus flows by mechanisms dependent upon the Prandtl number, $\sigma$. Solutions are obtained at $\sigma = 1$ for both the real annulus system and for the hypothetical " free annulus " system (free slip lateral boundaries). These solutions are compared with previously obtained solutions at $\sigma = 7$.

In the free annulus, the solution at $\sigma = 1$ differs radically from that at $\sigma = 7$. The $\sigma = 1$ solution appears to be essentially a finite amplitude mode due to Solberg instability whereas the solution at $\sigma = 7$ manifests a flow caused by the diffusive overturning mechanism.

The variation with $\sigma$ of the real annulus flow is not so fundamental but some differences in the dynamical structures are noted.

## 1. Introduction

Some numerical solutions for axisymmetric convection in annulus systems have been presented in a series of papers[4,5] which we shall refer to as Part 1, 2 and 3. The nature of the flows in the solutions was found to be critically dependent upon the assumed lateral boundary conditions. For this paper, it is convenient to define 2 annulus systems, one being the standard real annulus and the other being what we shall term a " free annulus " system in which the lateral boundaries are free slip surfaces. Both systems have a free slip upper surface and a no-slip base. The free annulus system is hypothetical but may be of geophysical significance because of the frontal type flows produced in it, see Part 3. The real annulus system with a rigid upper surface is not considered in this paper.

McIntyre[3] has shown how the dynamics throughout most of the free annulus flow can be interpreted as being essentially the same

as that of a flow at a finite amplitude stage of his diffusive overturning instability. The rôle of the diffusive overturning mechanism is not so important in real annulus flows whose dynamics are complex and have yet to be fully explained.

As examples of the 2 flow categories at $\sigma = 7$, we will refer to the solutions, A3 for the real annulus and A3B for the free annulus, which were discussed in Part 3. To examine how active the diffusive overturning mechanism is in the 2 flow types we recalculate the A3, A3B ($\sigma = 7$) solutions at $\sigma = 1$ by increasing the conductivity so that $\kappa = \nu$. The resulting flows which we denote as A3S, A3BS respectively, are deprived of the diffusive overturning mechanism which does not occur when $\sigma = 1$. The degree of similarity between the representative $\sigma = 1$ and $\sigma = 7$ solutions should therefore depend on how much the $\sigma = 7$ solutions rely on the diffusive overturning mechanism for their existence. (We cannot rule out the possibility that other $\sigma$ dependent mechanisms may also be present but they are thought to be secondary.)

It is found that the solution A3S for the real annulus at $\sigma = 1$ is essentially the same as A3 for $\sigma = 7$ although there are some differences in their dynamics. However, for the free annulus the solution A3BS for $\sigma = 1$ differs completely from A3B for $\sigma = 7$ and as will be seen it owes its existence to the classical Solberg instability mechanism. This result confirms the importance of the diffusive overturning mechanism in the dynamics of free annulus flows like A3B.

## 2. Equations and Parameters

We consider a fluid bounded by two co-axial cylinders of inner and outer radii $a$, $b$, respectively, and two parallel horizontal planes which are a distance $d$ apart. The container rotates at a constant rate $\mathbf{\Omega}$, where the rotation vector coincides with the vertical axis of the cylinders. Motion is considered relative to the solid rotation and is measured in cylindrical coordinates $r$, $z$ based on the axis, $r$ being radial and $z$ vertical. The variables $u$, $v$, $w$ denote velocity components in the zonal, radial and vertical directions. The perfectly conducting inner and outer lateral boundaries are held at different constant temperatures $T_a$ and $T_b$, respectively ($T_b > T_a$). This imposed horizontal temperature differential, $\Delta T = T_b - T_a$ drives

the fluid away from a state of solid rotation. The base ($z = 0$) and upper surface ($z = d$) are thermally insulating, i.e., $T_z = 0$.

The following definition of a Boussinesq liquid is taken: that density variations are negligible except in the buoyancy term and that the coefficients $\nu$, $\kappa$, $\beta$ of viscosity, heat diffusivity and thermal expansion are constants. We also take the centrifugal acceleration to be negligible compared with gravity: $\Omega^2 b/g \ll 1$. Then the governing equations may be written as follows:

$$\zeta_t + J\left(\psi, \frac{\zeta}{r}\right) = -\beta g T_r + 2u_z\left(\Omega + \frac{u}{r}\right) + \nu\left[\zeta_{zz} + \left\{\frac{1}{r}(r\zeta)_r\right\}_r\right] \tag{1}$$

$$u_t + \frac{1}{r}J(\psi, u) = \frac{\psi_z}{r}\left(2\Omega + \frac{u}{r}\right) + \nu\left[u_{zz} + \left(\frac{1}{r}(ru)_r\right)_r\right] \tag{2}$$

$$T_t + \frac{1}{r}J(\psi, T) = \kappa\left[T_{zz} + \frac{1}{r}(rT_r)_r\right] \tag{3}$$

$$\frac{1}{r}\psi_{zz} + \left(\frac{\psi_r}{r}\right)_r = -\zeta \tag{4}$$

$$m \equiv r(u + \Omega r) \tag{5}$$

where $J(\psi, \ ) \equiv \psi_r(\ )_z - \psi_z(\ )_r$ represents the convection term. The stream function $\psi$ and vorticity $\zeta$ describe the flow in the vertical $r, z$ plane and are defined by

$$rv = -\psi_z\,, \quad rw = \psi_r\,, \quad \zeta = v_z - w_r\,, \tag{6}$$

and $m$ is the absolute angular momentum.

The upper surface is taken as a free slip surface and the base as a rigid surface. There are two sets of lateral boundary conditions: (i) the real annulus system has non-slip sides and (ii) the free annulus has free slip sides by definition.

The equations are solved for the following set of parameters under the two boundary systems:

$$\begin{aligned} a &= 3.48\text{ cm},\ b = 6.02\text{ cm},\ d = 5.0\text{ cm},\\ \Delta T &= 29\,^\circ\text{C},\ \Omega = 1.342\text{ rad sec}^{-1},\ \bar{T} = 20\,^\circ\text{C},\\ \nu &= \kappa = 1.008 \times 10^{-2}\text{ cm}^2\text{ sec}^{-1},\ \beta = 2.054 \times 10^{-4}\,(^\circ\text{C})^{-1},\\ g &= 981\text{ cm sec}^{-2}. \end{aligned}$$

The associated external Rossby and Taylor numbers are $\pi_4 \equiv (\beta g \Delta T d)/[\Omega^2(b-a)^2] = 2.510$ and $\pi_5 \equiv 4\Omega^2(b-a)^5/(\nu^2 d) = 1.5 \times 10^6$.

Except for the value of $\kappa$ these are identical parameter values to those used in Part 3 for the A3 and A3B solutions for water. Equations (1)–(4) can be set up as a computational finite difference scheme and solutions obtained as detailed in Parts 1 and 3. The equations are integrated to a steady state from an initial state of isothermal solid rotation. A resolution of $40 \times 60$ grid points in the $r$, $z$ directions was used for the calculations.

(We might document here that the solution A3B has also been obtained under a different numerical scheme and program, that of Williams.[6] The differences between the two solutions is negligible, thus confirming the accuracy of the calculations.)

## 3. The Nature of the A3S Solution

The steady state solution A3S for the real annulus at $\sigma = 1$ is given in Fig. 1. The flow is not radically different from that of the A3 ($\sigma = 7$) solution, see Part 3.

The outward radial flow takes place in an Ekman layer on the base. The return cross-flow is not direct but makes a large dip down into the center of the fluid before rising to the top of the cold wall Associated with this dipping motion is the formation of two distinct secondary cells at the sidewalls. The meridional velocities in A3S are about double those of A3 in magnitude and the sidewall momentum layers are broader. The temperature fields of A3S and A3 are different in that only a weak thermal boundary layer forms on the cold cylinder in A3S whereas in A3 strong thermal boundary layers form on both cylinders, The zonal velocity has a positive upper and a negative lower flow. The magnitude of this flow exceeds that in

Figure 1. The steady state contours of (i) stream function, (ii) temperature, (iii) zonal velocity and (iv) absolute angular momentum of the case A3S. In all diagrams each variable is normalized with respect to its maximum and minimum values. The normalized maximum and minimum have the respective values of 1.0 and 0.0 and the other contours are at intervals of 0.1. The absolute value of any contour, e.g. $T$, may be determined from the relation $T = T_{\min} + \text{contour value} \times (T_{\max} - T_{\min})$. The absolute maximum and minimum values are (i) 0.0 and $-0.3147$ cm$^2$ sec$^{-1}$ for $\psi$, (ii) 34.5 and 5.5 °C for $T$, (iii) 3.144 and $-0.8414$ cm sec$^{-1}$ for $u$ and (iv) 48.63 and 16.25 cm$^2$ sec$^{-1}$ for $m$. The non-dimensional co-ordinate $r' \equiv (r-a)/(b-a)$ commences at the cold inner cylinder (on the left of each diagram) and $z' = z/d$.

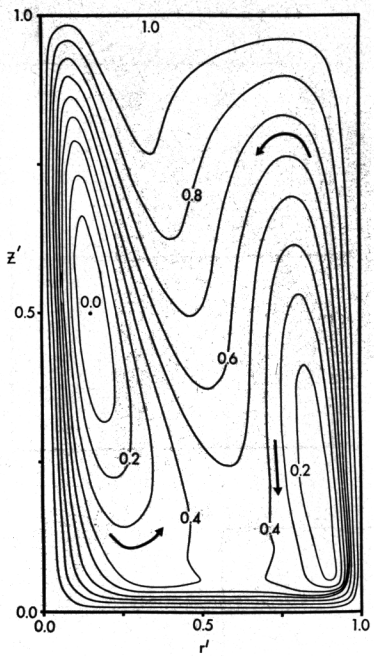
1.0
1.0
0.8
0.6
0.4
0.2
0.0
0.2
0.4
0.5
0.0
0.5
1.0
z'
r'

(i)

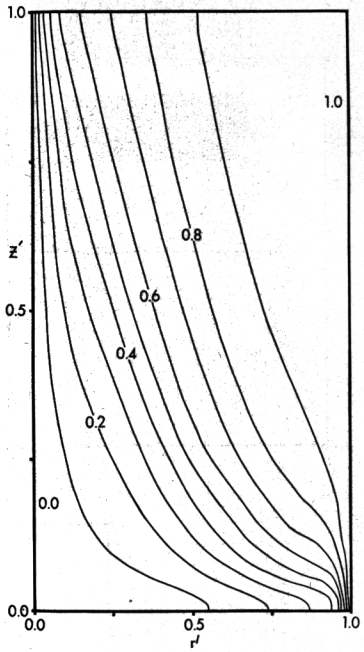
1.0
1.0
0.8
0.6
0.4
0.2
0.0
0.5
0.0
0.5
1.0
z'
r'

(ii)

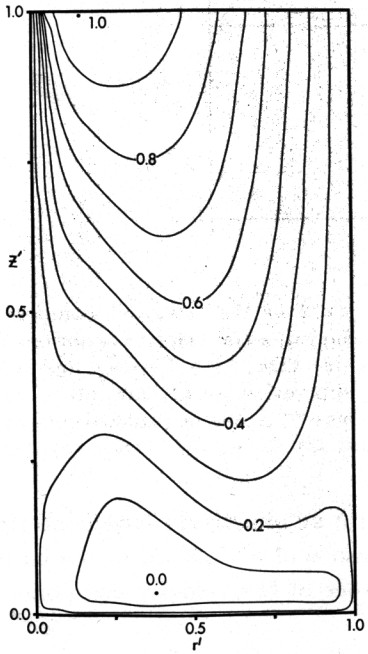
1.0
1.0
0.8
0.6
0.4
0.2
0.0
0.5
0.0
0.5
1.0
z'
r'

(iii)

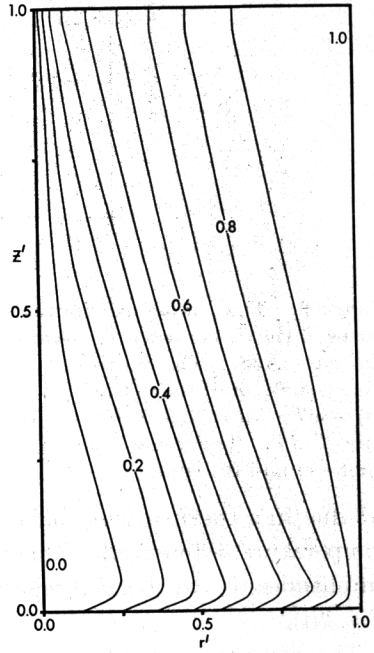
1.0
1.0
0.8
0.6
0.4
0.2
0.0
0.5
0.0
0.5
1.0
z'
r'

(iv)

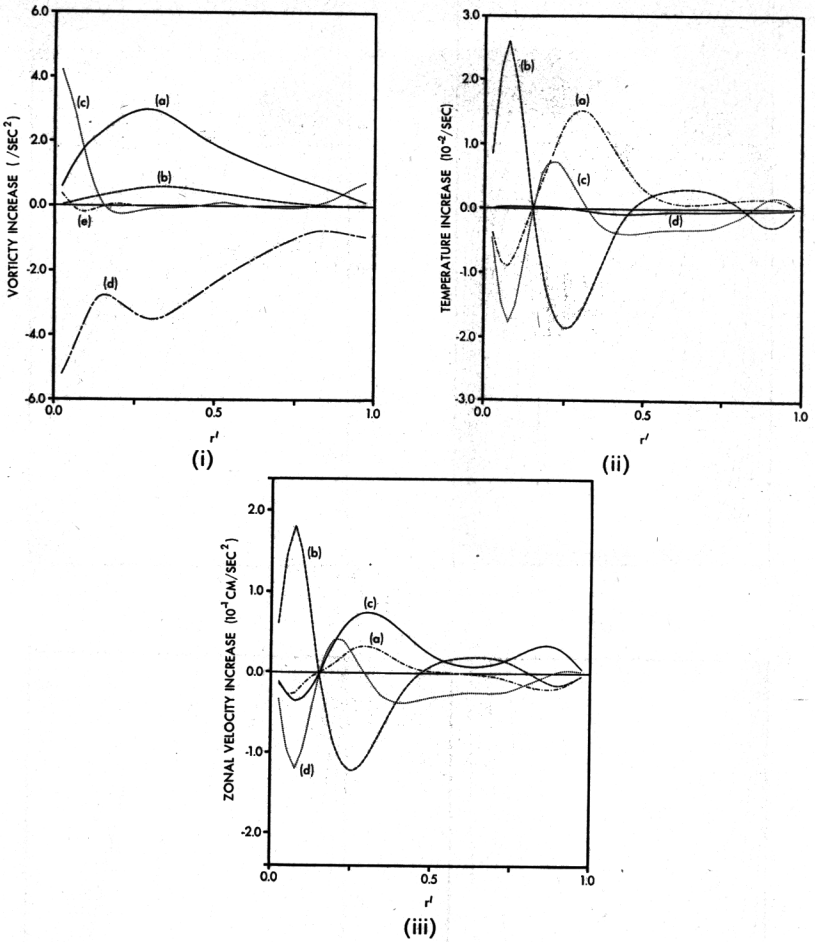


Figure 2. The radial distributions at $z = d/2$ of the balanced component terms of the (i) vorticity, (ii) temperature and (iii) zonal velocity equations for the case A3S. The vorticity terms are (a) $2\Omega u_z$, (b) $1/r(u^2)_z$, (c) $\nu\nabla^2\zeta$, (d) $-\beta g T_r$ and (e) $-J(\psi, \zeta/r)$. The temperature terms are (a) $-vT'_r$, (b) $-wT'_z$, (c) $\kappa(T'_{rr} + T'_r/r)$ and (d) $\kappa T'_{zz}$ where $T'$ is the normalized temperature $T/\Delta T$. The zonal velocity terms are (a) $-vu_r$, (b) $-wu_z$, (c) $(2\Omega + u/r)(-v)$ and (d) $\nu\nabla^2 u$.

A3 due to a thermal wind balance with an effectively larger internal temperature differential. This increase is also reflected in the larger amplitudes of the thermal wind balance of the velocity components Fig. 2(i).

The component balances, Fig. 2, tell us which of the dynamical

mechanisms are active in the formation of the A3S flow. In these diagrams (and those of Fig. 4) the convective terms are given in the form of e.g. $-wT_z$ rather than as $-(wT)_z$, the form used in earlier papers. Although these figures give the balances at $z = d/2$ only they do provide a good representation of the interior dynamical structure.

The vorticity balance of the interior is essentially a thermal wind balance, Fig. 2(i), with a modification by viscous and nonlinear processes. As noted, the amplitude of this balance is larger than that of the comparable balance for the A3 solution.

In the temperature balance, Fig. 2(ii), the separate components of the convection and conduction processes are given. The smallness of the vertical diffusion reflects the linearity of the isotherms at mid-height. The Nusselt number, defined as in Part 1, has a value of 2.20 which is well below the value of 8.25 for the A3 solution. This reflects the difficulty the fluid seems to have in getting across the upper region and accomplishing the heat transfer.

The zonal velocity balance, Fig. 2(iii), is complex. Viscous effects are important throughout most of the flow, as they are for the A3 solution. However, we note that in the region between $r' = 0.2$ and 0.4 viscous effects are secondary to a balance between Coriolis and inertia terms i.e. angular momentum is conserved in this region and the flow is parallel to the $m$ contours.

## 4. The Nature of the A3BS Solution

The steady state solution A3BS ($\sigma = 1$) for the free annulus system with its free slip lateral boundaries displays characteristics not met in other solutions, Fig. 3.

The meridional velocity field consists of a large, almost vertical, direct cell in the inner half of the fluid together a weaker, smaller indirect cell near the bottom of the hot wall. The velocities in all these cells are small. The cause of this motion will be discussed in Sec. 5.

The temperature field has only a weak vertical variation although it is not entirely conductively determined. There is a small radial variation linked with the cell motion. The zonal velocity is principally a function of height only and displays only a weak radial variation. The angular momentum contours are linear, Fig. 3(iv).

The vorticity component balance, Fig. 4(i), displays a thermal

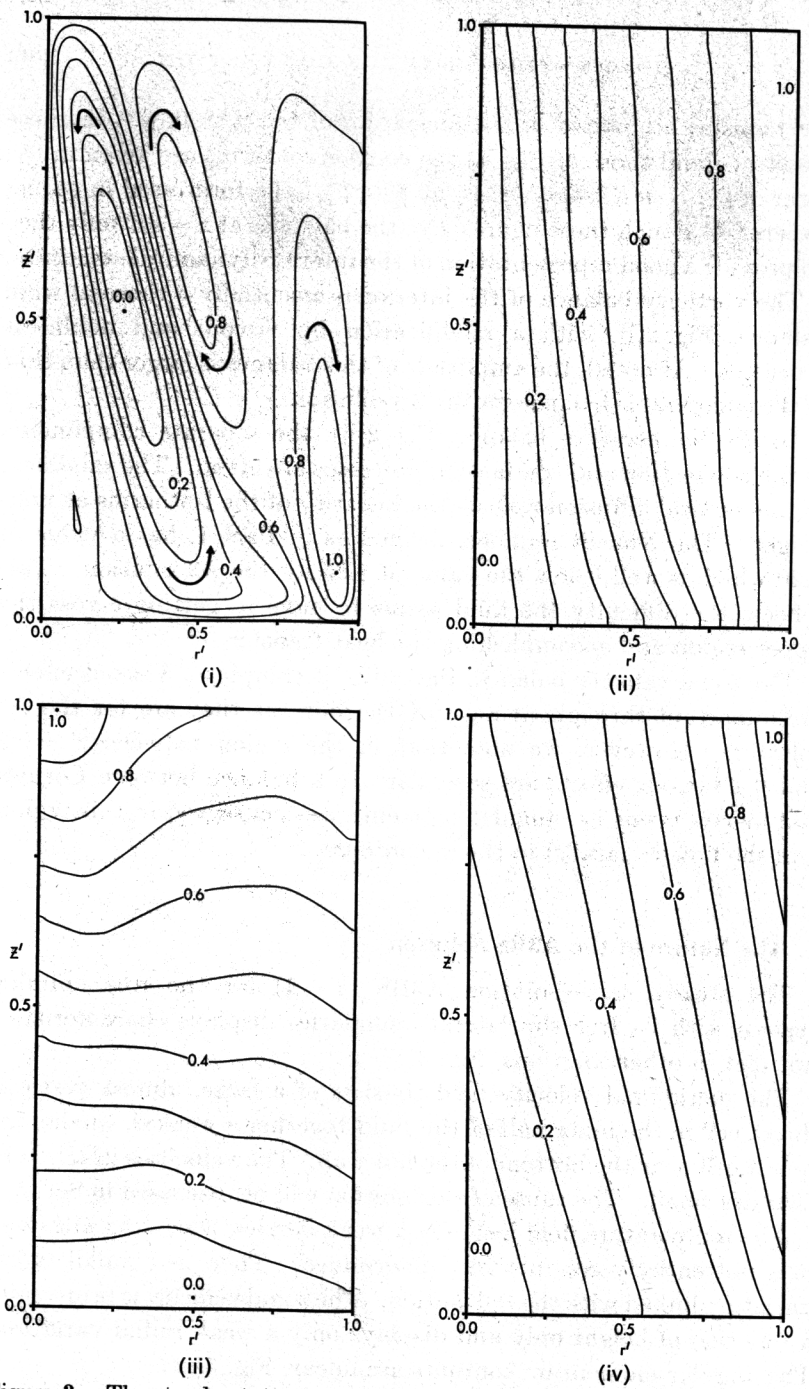


Figure 3. The steady state contours for case A3BS. The absolute maximum and minimum values are (i) 0.03572 and $-0.08291$ cm$^3$ sec$^{-1}$ for $\psi$, (ii) 34.5 and 5.5 °C for $T$, (iii) 3.896 and $-0.06804$ cm sec for $u$ and (iv) 67.83 and 16.25 cm$^3$ sec$^{-1}$ for $m$.

wind balance between the buoyancy and Coriolis terms that has an appreciable modification by the nonlinear terms. These main terms have little radial variation.

The amplitude of the temperature components, Fig. 4(ii), is small compared to for example A3S ($\frac{1}{4}$ of values) reflecting the conductive nature of the temperature field. The horizontal conduction term that we see in this balance $\kappa(T_{rr}+(1/r)T_r)$ is not a complete measure of the conductive nature but indicates the departure of the temperature field from a purely conductive variation of $T \propto \log r'$. The

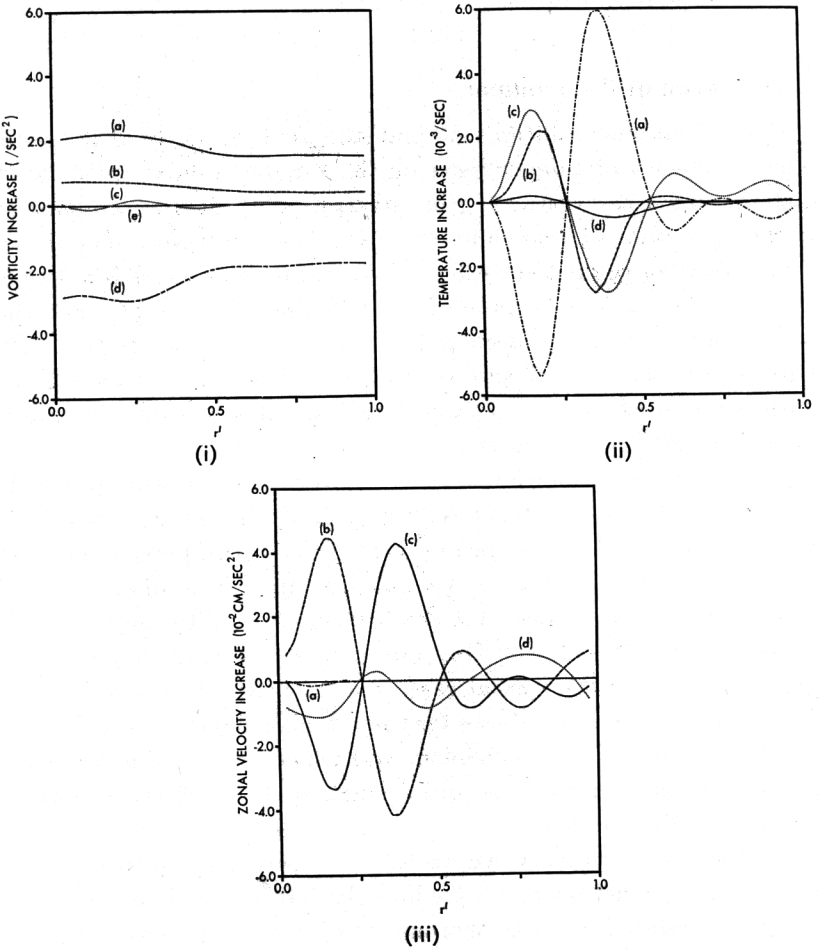


Figure 4. The component balances of case A3BS.

Nusselt number, 1.057 for this flow, indicates more clearly the low level of convective heat transfer.

The vertical inertia component and the Coriolis term dominate the balance of the zonal velocity equation, Fig. 4(iii), indicating that angular momentum is conserved in this flow. The viscous term acts as a modifying force but the horizontal inertia component is negligible.

The predominant Coriolis-inertia balance most clearly distinguishes this flow, which is due to the classical Solberg mechanism, from flows due to the diffusive overturning mechanism, such as A3B, which have a Coriolis-viscous balance.

## 5. Discussion of the Solutions

The real annulus solutions A3 and A3S are essentially of the same type. This lack of a dependence on the Prandtl number must mean that the diffusive overturning mechanism is relatively unimportant in the dynamics of real annulus flows. An interpretation of the dynamics of these flows in terms of analytical expressions is not easy and no attempt will be made here. We note, however, that the angular momentum contours and isotherms, Fig. 1, shows that A3S is free of the classical Solberg instability. Thus that mechanism can be discounted for the $\sigma = 1$ case of real annulus flows in this range of Rossby and Taylor numbers.

The free annulus solution at $\sigma = 1$, A3BS, has a relatively simple structure and can be interpreted analytically in terms of Solberg's instability theory for a baroclinic vortex. The component terms of Fig. 4 with their Coriolis-inertia balance and sinusoidal variation provide the best evidence that the Solberg instability mechanism is responsible for this flow. The linear theory is most conveniently applied by taking the special case, $\sigma = 1$, of McIntyre's analysis.[2] This form of the theory allows for the diffusion effects which modify the Solberg instability mechanism and which lead to the definition of a theoretical length scale and a small scale cutoff, two features absent in Solberg's theory.

In McIntyre's[2] theory we are given a baroclinic vortex having mean basic $\bar{C}$, $\bar{T}$ fields which vary linearly and uniformly in space and which are related by the thermal wind formula. Axisymmetric motions can grow exponentially from rest within this vortex pro-

vided that the isotherms are more vertically inclined than the $\bar{C}$ contours (the latter are related to the angular momentum contours). The solution A3BS, Fig. 3, clearly has this unstable configuration.

The solution in Fig. 3 can be regarded as being made up of the basic fields plus the disturbance at some finite amplitude. The $\psi$ field is due to the disturbance only. To obtain the details of the instability, we must first extract plausible basic $\bar{C}$, $\bar{T}$ distributions. To do this the solution is averaged and an adjustment to the Cartesian co-ordinates of the theory is made in the manner detailed in the Appendix of McIntyre.[3] This procedure yields values for the angles, $\bar{\Gamma}$, $\bar{\Theta}$ made with the vertical by the $\bar{C}$, $\bar{T}$ contours respectively as $\tan\bar{\Gamma} = 0.2090$ and $\tan\bar{\Theta} = 0.0561$. These are small angles.

The characteristic equation for the growth of a disturbance of the form $\exp(ik(r\cos\phi + z\sin\phi) + \omega t)$, when $\sigma = 1$, is

$$(\omega + k^2)((\omega + k^2)^2 + (\mathscr{G} + \mathscr{I})) = 0, \tag{7}$$

where

$$\mathscr{G} \equiv s\frac{\cos\phi}{\cos\bar{\Theta}}\sin(\bar{\Theta} - \phi),\quad \mathscr{I} \equiv s\frac{\sin\phi}{\sin\bar{\Gamma}}\sin(\phi - \bar{\Gamma}),\quad s \equiv \operatorname{sgn}(\tan\bar{\Gamma}). \tag{8}$$

$\mathscr{G}$ and $\mathscr{I}$ represent gravitational and inertial restoring forces respectively and are functions of $\phi$, the inclination of the disturbance streamlines to the vertical (see McIntyre[2] for full details). The disturbance is associated with the root

$$\omega = -i(\mathscr{G} + \mathscr{I})^{1/2} - k^2 \tag{9}$$

of Eq. (7). This root is positive for all values of $\phi$ as $\mathscr{G} \simeq \bar{\Theta} - \bar{\Gamma} < 0$, $\mathscr{I} \simeq 0$ for the small angles involved in A3BS. The trivial root $\omega = -k^2$ is a degenerate form of that root which gives the diffusive instability when $\sigma \neq 1$.

For a fixed wave number $k$ the maximum growth rate for this root occurs at an inclination $\phi$ given by

$$\frac{\mathrm{d}}{\mathrm{d}\phi}(\mathscr{G} + \mathscr{I}) = 0,$$

i.e.

$$2\cot 2\phi = \cot\bar{\Gamma} - \tan\bar{\Theta}. \tag{10}$$

For small angles this gives $\phi \simeq \bar{\Gamma}$. The solution A3BS does have streamlines that lie parallel to the angular momentum contours in

this way. Thus the streamfunction of the solution is aligned in that direction which provides (theoretically) the maximum growth rate for a given $k$.

The absolute maximum growth rate would have $k = 0$ but as this is not observed we conclude that $k$ must be determined by the boundary constraints instead. There is a distribution of about 5/2 wavelengths in the component balances, Fig. 4. This suggests a value for the activating $k$ of $k = 5\pi\delta/(b-a)$ where a timescale $\tau = (\beta g \bar{T}_r)^{-1/2}$ and a length scale $\delta = (\nu\tau)^{1/2}$ have values close to those of A3B as calculated by McIntyre.[3]

Thus the dimensionless growth rate corresponding to the solution A3BS is

$$\omega = (\bar{\Gamma} - \bar{\Theta})^{1/2} - k^2 = 0.39 - 0.27 = 0.12$$

This growth rate is about four times larger than that for the diffusive instability associated with A3B. The substantial $k^2$ contribution indicates that this disturbance is near the small scale cut-off. It is important, however, to remember that the solution is a steady state solution so the correspondence to the theoretical instability is limited. We could perhaps best regard the solution as being at that stage where the exponential growth has been balanced by effects omitted by linear theory.

## 6. Conclusions

The solutions at $\sigma = 1$ and $\sigma = 7$ lead us to believe that Prandtl number effects are only a minor contributor to the mechanics of the real annulus (as the system is defined in this paper) but for the free-annulus system they are of major importance. The diffusive overturning mechanism is the mechanism of the Prandtl number effects and is responsible for the A3B flow.

The numerical solution A3BS is an example of the classical Solberg instability of a baroclinic vortex (with some modification by diffusion).

## Acknowledgement

I am indebted to Michael McIntyre for the stimulating discussions that led to making this study.

## REFERENCES

1. McIntyre, M. E., " The axisymmetric convective regime for a rigidly bounded rotating annulus," *J. Fluid Mech.* **32**, 625–655 (1968).
2. McIntyre, M. E., " Diffusive destabilization of the baroclinic circular vortex," *Geophysical Fluid Dynamics* **1**, 19 (1970).
3. McIntyre, M. E., " Role of diffusive overturning in nonlinear axisymmetric convection in a differentially heated rotating annulus," *Geophysical Fluid Dynamics*, **1**, 59 (1970).
4. Williams, G. P., " Thermal convection in a rotating fluid annulus," Part 1, 2 *J. Atmos. Sci.* **24**, 144–174 (1967).
5. Williams, G. P., " Thermal convection in a rotating fluid annulus," Part 3. *J. Atmos. Sci.* **25**, 1035–1045 (1968).
6. Williams, G. P., " Numerical integration of the three dimensional Navier–Stokes equations for incompressible flow," *J. Fluid Mech.* **37**, 727–750 (1969).